Chapter

Biomechanical Model Improving Alzheimer's Disease

Eliete Biasotto Hauser, Wyllians Vendramini Borelli and Jaderson Costa da Costa

Abstract

The aim this study is to describe the algorithms of kinetic modeling to analyze the pattern of deposition of amyloid plaques and glucose metabolism in Alzheimer's dementia. A two-tissue reversible compartment model for Pittsburgh Compound-B ($[^{11}C]PIB$) and a two-tissue irreversible compartment model for $[^{18}F]$2-fluoro-2-deoxy-D-glucose ($[^{18}F]FDG$) are solved applying the Laplace transform method in a system of two first-order differential equations. After calculating a convolution integral, the analytical solutions are completely described. In order to determine the parameters of the model, information on the tracer delivery is needed. A noninvasive reverse engineer technique is described to determine the input function from a reference region (carotids and cerebellum) in PET image processing, without arterial blood samples.

Keywords: noninvasive input function, Laplace transform, kinetic modeling, radiotracer, positron emission tomography (PET), reference region, region of interest, time activity curve

1. Introduction

Positron emission tomography (PET) [1, 2], is a functional imaging technology that visualizes physiological changes through the administration of radiopharmaceutical molecular tracers into living systems. PET with measures the local concentration of a tracer in the region of interest (ROI) or target tissue.

PET with $[^{11}C]PIB$ and $[^{18}F]FDG$ radiotracers are widely used in the clinical setting for patients with neurodegenerative diseases like Alzheimer's disease. The $[^{18}F]FDG$-PET indirectly measures neuronal metabolism, subsequently allowing the identification of brain regions with increased or decreased activity. Individuals with progressive amnestic dementia show a specific pattern of FDG uptake that distinguishes their brains from other types of pathologies. Thus, this technique directly impacts the treatment selected for this patient. However, this technique is still under study to improve its accuracy power and to decrease patient discomfort undergoing this diagnostic tool.

Cognitive aging is also a subject of interest of PET studies. This technique can be used to investigate abnormal binding occurs in clinically normal individuals, prior to the development of cognitive changes. Higher binding in nondemented subjects suggests that $[^{11}C]PIB$ amyloid imaging may be sensitive for detection of a preclinical Alzheimer's disease state. Age-related cognitive changes impact the brain functioning

and subsequently neuronal activity. Frontal and medial temporal regions are particularly vulnerable for the aging process. Nonetheless, a group of elderly named SuperAgers exhibit exceptional memory ability and a specific brain signature [3–7]. SuperAgers appear to maintain neuronal activity throughout the aging process, showing stable neuronal activity in the frontal lobe when compared with normal agers.

Mathematical modeling seeks to describe the processes of distribution and elimination through compartments, which represent different regions (for example, the vascular space, interstitial, intracellular) or different chemical stages. Noninvasive methods have been used successfully in PET image studies [8–13].

In order to determine the parameters of the model, information on the tracer delivery is needed in the form of the input function that represents the time-course of tracer concentration in the arterial blood or plasma is non-invasively obtained by non-linear regression [14], from the time-activity curve in a reference region (carotids and cerebellum).

The Laplace transform is used to generate the exact solution solutions of the $[^{11}C]PIB$ two-tissue reversible compartment model, [15], and $[^{18}F]FDG$ two-tissue irreversible compartment model, [16, 17], applying the Laplace transform method in a system of two first order differential equations. From a reference region (carotids and cerebellum) the technique allows to estimate the concentration in each compartment of the region of interest, illustrated in **Figure 1**.

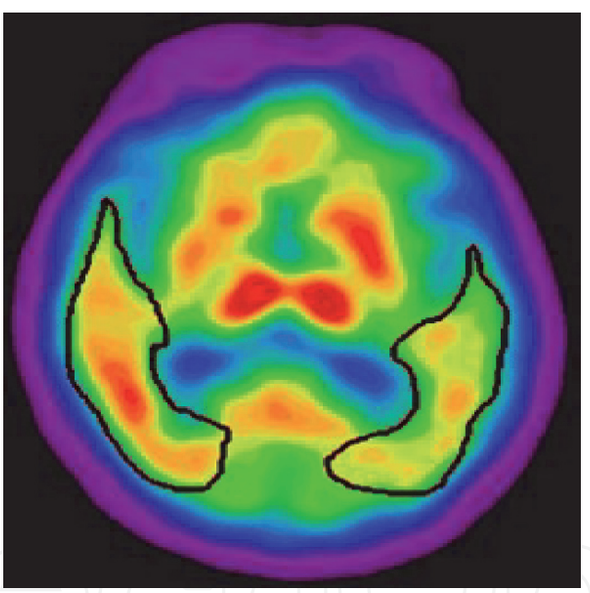

Figure 1.
Region of interest outlined in temporal areas bilaterally in an axial slice.

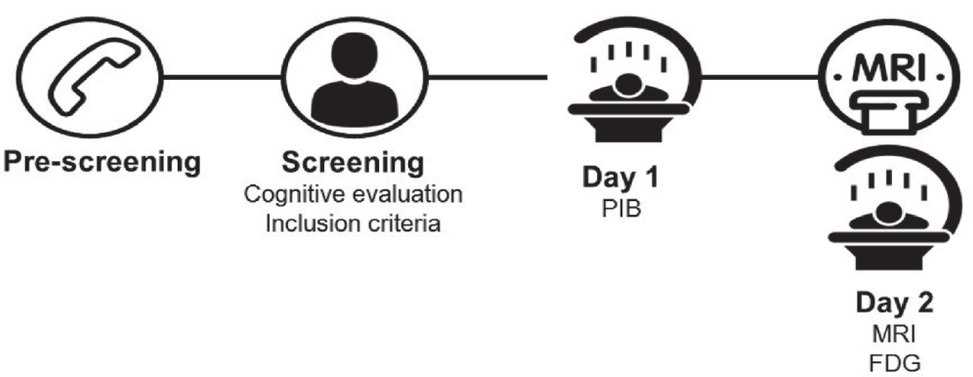

Figure 2.
SuperAgers project study protocol.

1.1 Image analysis and data generation

Data used in this work was obtained with $[^{18}F]FDG$ and $[^{11}C]PIB$ synthesized by the Cyclotron at the Instituto do Cérebro (InsCer/BraIns) at the Pontifical Catholic University of Rio Grande do Sul PUCRS, in studies (**Figure 2**) approved by medical ethics committee with *PET*/*CT* imaging.

Using software PMOD, the 3D Gaussian pre-processing tool is used to make decay, attenuation, scatter and dead time corrections.

1.2 Effective dose injected (EDI) and half-life

According [1], the effective dose injected can be calculated as:

$$EDI = C_a^i e^{-\frac{\ln 2}{t_{1/2}}(t_0 - t_i)} - C_a^e e^{-\frac{\ln 2}{t_{1/2}}(t_e - t_0)} \tag{1}$$

where C_a^i is the dose measured before injection at time t_i, C_a^i is the rest dose after injection measured at time t_e and $t_{1/2}$ is the half-life of the tracer.

The radioactivity of $[^{11}C]PIB$ decays with a half-life of $t_{1/2}$ = 20 min and of $[^{18}F]$ *FDG* with a half-life of 109.7 min.

2. Models compartments

Mathematical modeling seeks to describe the processes of distribution and elimination through compartments, which represent different regions (for example, the vascular space, interstitial, intracellular) o different chemical stages.

Transferring rate from one compartment to another, is proportional to concentration in the compartment of origin. Compartmental model is an important kinetic modeling technique used for quantification of PET. Each compartment is characterized by the concentration within it as a function of time. The physiological and metabolic transport processes are described mathematically by the analysis of mass balance equations.

A compartment model is represented by a system of differential equations, where each equation represents the sum of all the transfer rates to and from a specific compartment:

$$\frac{d}{dt}C_i(t) = \sum_{j=1, j\neq i}^{N} \left[K_{ij}C_j(t) - K_{ji}C_i(t)\right], \tag{2}$$

where $C_i(t)$ is the concentration of radioactive tracer in compartment i, N is the number of sections of the model, K_{ji} is the rate constant for transfer from compartment j to compartment i.

Figure 3 illustrates a reversible compartment model, that is be used to investigated the $[^{11}C]PIB$ metabolism, [15], because this tracer enters a reference region and since it does not find amyloid plaques to bind it leaves rapidly.

The irreversible two compartment model (**Figure 2** with $k_4 = 0$) is used for description of tracer $[^{18}F]FDG$, [16, 17], which first enter a free compartment, C1, and is then metabolized irreversibly in the second compartment C2.

In order to determine the parameters of the model, it is necessary to have information about the tracer delivery in the form of an input function representing the time-course of tracer concentration in arterial blood or plasma.

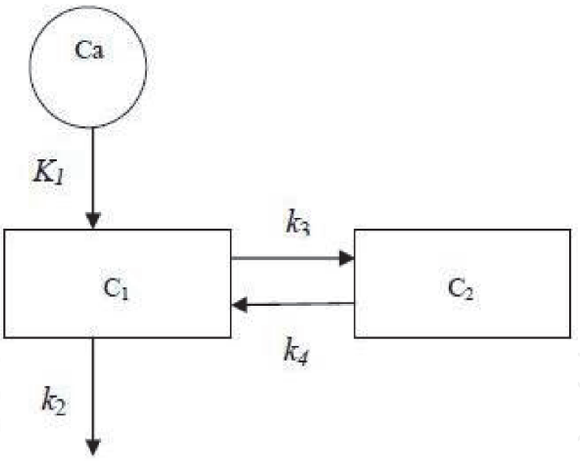

Figure 3.
A schematic diagram of a reversible two compartments model to illustrate the flux of tracer between blood (Ca) and and two tissues (C1 and C2).

2.1 Estimation of rate constants

In order to estimate the parameters k_{ij}, k_{ji}, a nonlinear regression problem is solved using the Levenberg-Marquardt method [18, 19]. The sensitivity equations are generated partially deriving Eq. (2) with respect to the parameters k_{ij}, k_{ji}

$$\begin{cases} \dfrac{\partial}{\partial K_{ij}}\left(\dfrac{d}{dt}C_i(t) = \displaystyle\sum_{j=1,j\neq i}^{N}\left[K_{ij}C_j(t) - K_{ji}C_i(t)\right]\right) \\ \dfrac{\partial}{\partial K_{ji}}\left(\dfrac{d}{dt}C_i(t) = \displaystyle\sum_{j=1,j\neq i}^{N}\left[K_{ij}C_j(t) - K_{ji}C_i(t)\right]\right) \end{cases} \tag{3}$$

Over which region of interest (ROI) is defined discrete TAC using the image processing. The Jacobian matrix it consists of the column vectors whose values resulting from the numerical integration of the sensitivity equations with respect to time.

3. Two-tissue reversible compartment model of [^{11}C]*PIB*

The mathematical model for the representation of the dynamics of [^{11}C]*PIB* radiotracer, [11, 15, 20], is expressed by the system of two differential equations:

$$\begin{cases} \dfrac{dC_1}{dt} = K_1C_a(t) - (k_2 + k_3)C_1(t) + k_4C_2(t) \\ \dfrac{dC_2}{dt} = k_3C_1(t) - k_4C_2(t) \\ C_1(0) = 0, C_2(0) = 0. \end{cases} \tag{4}$$

where $C_a(t)$ is the arterial input function (AIF) considered to be known, $C_1(t)$ and $C_2(t)$ are, respectively, the concentration within the non-displaceable and displaceable compartments and K_1 and k_2, k_3, k_4 are kinetic rate constants which have to be determined.

The Laplace transform with respect to t is applied to solve the system of differential equations Eq. (4), with the notation

$$\mathcal{L}\{C_i(t)\} = \overline{C}_i(s) = \int_0^\infty e^{-st} C_i(t)\,dt$$

and

$$\mathcal{L}\left\{\frac{d\,C_k(t)}{dt}\right\} = s\,\overline{C}_i(s) - C_i(0).$$

An algebraic system is obtained

$$\begin{cases} (s + k_2 + k_3)\,\overline{C}_1(s) - k_4\,\overline{C}_2(s) = K_1\,\overline{C}_a(s) \\ -k_3\,\overline{C}_1(s) + (s + k_4)\,\overline{C}_2(s) = 0 \end{cases}, \tag{5}$$

that can be written in matrix form as

$$\begin{bmatrix} s + k_2 + k_3 & -k_4 \\ -k_3 & s + k_4 \end{bmatrix} \begin{bmatrix} \overline{C}_1(s) \\ \overline{C}_2(s) \end{bmatrix} = \begin{bmatrix} K_1\,\overline{C}_a(s) \\ 0 \end{bmatrix}. \tag{6}$$

The solution of the algebraic system (6) is

$$\begin{bmatrix} \overline{C}_1(s) \\ \overline{C}_2(s) \end{bmatrix} = \begin{bmatrix} s + k_2 + k_3 & -k_4 \\ -k_3 & s + k_4 \end{bmatrix}^{-1} \begin{bmatrix} K_1\,\overline{C}_a(s) \\ 0 \end{bmatrix}. \tag{7}$$

The inverse matrix is

$$\begin{bmatrix} s + k_2 + k_3 & -k_4 \\ -k_3 & s + k_4 \end{bmatrix}^{-1} = \frac{1}{(s + k_2 + k_3)(s + k_4) - k_3 k_4} \begin{bmatrix} s + k_4 & k_4 \\ k_3 & s + k_2 + k_3 \end{bmatrix}. \tag{8}$$

Therefore,

$$\begin{aligned} \overline{C}_1(s) &= \frac{(s + k_4)\,K_1\,\overline{C}_a(s)}{s^2 + (k_2 + k_3 + k_4)s + k_2 k_4} \\ \overline{C}_2(s) &= \frac{k_3 K_1\,\overline{C}_a(s)}{s^2 + (k_2 + k_3 + k_4)s + k_2 k_4} \end{aligned} \tag{9}$$

Using the inverse Laplace in Eq. (9), results

$$\begin{aligned} C_1(t) &= \mathcal{L}^{-1}\left\{\frac{(s + k_4)\,K_1\,\overline{C}_a(s)}{s^2 + (k_2 + k_3 + k_4)s + k_2 k_4}\right\} \\ C_2(t) &= \mathcal{L}^{-1}\left\{\frac{k_3 K_1\,\overline{C}_a(s)}{s^2 + (k_2 + k_3 + k_4)s + k_2 k_4}\right\}. \end{aligned} \tag{10}$$

Now, the proprieties inverse Laplace transform are used, considering * to denote the convolution[1].

[1] The property of commutativity is valid in convolution operation for Laplace transform of $f(t)$ and $g(t)$ functions, defined by $f(t) * g(t) = \int_0^t f(u)g(t-u)\,du = \int_0^t f(t-u)g(u)du$.

$$C_1(t) = \pounds^{-1}\left\{\frac{(s+k_4)}{s^2+(k_2+k_3+k_4)s+k_2k_4}\right\} * K_1\pounds^{-1}\{\overline{C}_a(s)\}$$
$$C_2(t) = \pounds^{-1}\left\{\frac{k_3}{s^2+(k_2+k_3+k_4)s+k_2k_4}\right\} * K_1\pounds^{-1}\{\overline{C}_a(s)\}. \quad (11)$$

Then,

$$C_1(t) = K_1\pounds^{-1}\left\{\frac{s+k_4}{s^2+(k_2+k_3+k_4)s+k_2k_4}\right\} * C_a(t)$$
$$C_2(t) = K_1\pounds^{-1}\left\{\frac{k_3}{s^2+(k_2+k_3+k_4)s+k_2k_4}\right\} * C_a(t). \quad (12)$$

$$\frac{s+k_4}{s^2+(k_2+k_3+k_4)s+k_2k_4} = \frac{A}{s-s_1}+\frac{B}{s-s_2}$$
$$\frac{k_3}{s^2+(k_2+k_3+k_4)s+k_2k_4} = \frac{C}{s-s_1}+\frac{D}{s-s_2} \quad (13)$$

In Eq. (13) s_1 and s_2 are the roots of $s^2+(k_2+k_3+k_4)s+k_2k_4=0$, dependent on transport constants k_2, k_3, and k_4. The parameters A, B, C, and D are obtained by partial fraction decomposition technique. Then, because that the inverse Laplace transforms are simply linear combinations of exponential functions with the exponents s_1 and s_2 depending on k_2, k_3, and k_4. Applying the linearity property of the inverse Laplace transform is obtained

$$C_1(t) = K_1\{Ae^{s_1t}+Be^{s_2t}\} * C_a(t)$$
$$C_2(t) = K_1\{Ce^{s_1t}+De^{s_2t}\} * C_a(t) \quad (14)$$

The analytical solution of the reversible two-compartment model for $[^{11}C]PIB$ (4) is

$$C_1(t) = K_1\left\{Ae^{s_1t}\int_0^t e^{-s_1u}C_a(u)du + Be^{s_2t}\int_0^t e^{-s_2u}C_a(u)du\right\}$$
$$C_1(t) = K_1\left\{Ce^{s_1t}\int_0^t e^{-s_1u}C_a(u)du + De^{s_2t}\int_0^t e^{-s_2u}C_a(u)du\right\} \quad (15)$$

In Eq. (15), it is visible the importance of construction of input function $C_a(t)$ in order to make it possible to calculate the integral

$$I = \int_0^t e^{s_i u}\,C_a(u)\,du. \quad (16)$$

4. Two-tissue irreversible compartment model of $[^{18}F]FDG$

$[^{18}F]FDG$ is a glucose analogue used to evaluate brain's metabolic activity in vivo through positron emission tomography with computed tomography (PET/CT). The irreversible two-compartment model for $[^{18}F]FDG$ is used for description of this tracer, which is first entering a free compartment, C1, and is then metabolized irreversibly in the second compartment C2, [16].

$$\begin{cases} \dfrac{d}{dt}C_1(t) = K_1 C_a(t) - (k_2 + k_3) C_1(t) \\ \dfrac{d}{dt}C_2(t) = k_3 C_1(t) \\ C_1(0) = 0, C_2(0) = 0 \end{cases}, \tag{17}$$

where $C_a(t)$ is the input function and is considered to be known, $C_1(t)$ and $C_2(t)$ are the concentration in C1 and C2 compartments, respectively, and K_1, k_2, k_3 are positives proportionality rates describing, the tracer influx into and the tracer outflow from the compartment (transport constants).

Similarly to that developed in the previous section, considering $k_4 = 0$, applying the Laplace transform with respect to t in Eq. (17), appear the algebraic system

$$\begin{cases} (s + k_2 + k_3)\overline{C}_1(s) = K_1 \overline{C}_a(s) \\ -k_3 \overline{C}_1(s) + s\overline{C}_2(s) = 0 \end{cases}. \tag{18}$$

Eq. (18) is represented matrically

$$\begin{bmatrix} \overline{C}_1(s) \\ \overline{C}_2(s) \end{bmatrix} = \begin{bmatrix} s + k_2 + k_3 & 0 \\ -k_3 & s \end{bmatrix}^{-1} \begin{bmatrix} K_1 \overline{C}_a(s) \\ 0 \end{bmatrix}. \tag{19}$$

$$\begin{bmatrix} \overline{C}_1(s) \\ \overline{C}_2(s) \end{bmatrix} = \frac{1}{s(s + k_2 + k_3)} \begin{bmatrix} s & 0 \\ k_3 & s + k_2 + k_3 \end{bmatrix} \begin{bmatrix} K_1 \overline{C}_a(s) \\ 0 \end{bmatrix}. \tag{20}$$

Then,

$$\begin{aligned} \overline{C}_1(s) &= \frac{K1\overline{C}_a(s)}{s + k_2 + k_3} \\ \overline{C}_2(s) &= \frac{k_3 K_1 \overline{C}_a(s)}{(s + k_2 + k_3)s} = \frac{k_3 C_1(s)}{s} \end{aligned} \tag{21}$$

$$\begin{aligned} C_1(t) &= \pounds^{-1}\left\{ \frac{K_1 \overline{C}_a(s)}{(s + k_2 + k_3)} \right\} = K_1 \pounds^{-1}\left\{ \frac{1}{(s + k_2 + k_3)} \right\} * \pounds^{-1}\{\overline{C}_a(s)\} \\ C_2(t) &= \pounds^{-1}\left\{ \frac{k_3 \overline{C}_1(s)}{s} \right\} = k_3 * \pounds^{-1}\{\overline{C}_1(s)\}. \end{aligned} \tag{22}$$

The representation Eq. (22) implies that

$$\begin{aligned} C_1(t) &= K_1 e^{-(k_2+k_3)t} * C_a(t) = K_1 \int_0^t e^{-(k_2+k_3)(t-u)} C_a(u) du \\ C_2(t) &= k_3 * C_1(t) = k_3 \int_0^t C_1(u) du. \end{aligned} \tag{23}$$

Then, with $k_2 + k_3 > 0$, the analytical solution of the irreversible two compartment model for $[^{18}F]FDG$ Eq. (17) is

$$\begin{aligned} C_1(t) &= K_1 e^{-(k_2+k_3)t} \int_0^t e^{(k_2+k_3)u} C_a(u) du \\ C_2(t) &= k_3 \int_0^t C_1(u) du. \end{aligned} \tag{24}$$

It is important now to choose a suitable model to represent the input function $C_a(t)$, which makes it possible to calculate the integral $\int_0^t e^{(k_2+k_3)u} K_1 C_a(u)du$.

4.1 The input concentration

The knowledge of the input function is mandatory in quantifying by compartmental kinetic modeling. The radioactivity concentration of arterial blood can be measured during the course of the scan collecting blood samples.

Several techniques have been proposed for obtaining input function. [9] present five different forms to measure this data and [8] eight methods for the estimation image input function in dynamic $[^{18}F]FDG$ PET human brain. The image arterial input function provides data that are similar to arterial blood input methods and can be used to quantify, noninvasively, in PET studies, according to previous studies [8, 10, 13, 15, 20]. This technique calculate the input function using linear and nonlinear regression applied in a applied to a discrete set of data, discrete time activity curve (TAC) of reference region [11].

4.2 Input function derived of PET image

The dynamics of the radiotracer, [11, 17], on the reference region is governed by the differential equation

$$\frac{dC_r}{dt} = K_1' C_a(t) - k_2' C_r(t) \tag{25}$$

where $C_a(t)$ is the concentration of the radiotracer in the arterial blood, $C_r(t)$ is the concentration of the radiotracer in the reference region and $K_1' > 0$ and $k_2' > 0$ are the proportionality rates describing, respectively, the tracer influx into and the outflow from the reference tissue.

$C_r(t)$ is constructed from a TAC of a reference region [11].

After this, deriving $C_r(t)$ we obtain $C_a(t)$, which is the AIF, using

$$C_a(t) = \frac{1}{K_1'}\frac{dC_r}{dt} + \frac{k_2'}{K_1'} C_r(t) \tag{26}$$

The transport of the radiotracer across of arterial blood is very fast in the first few minutes and then decreases slowly. Then, it may be appropriate to estimate the $C_r(t)$ in a few stages as piecewise function, [16]. This is defined for three stages in the equation

$$\begin{aligned} C_r(t) = {} & (H(t-t_0) - H(t-t_1))C_{rf}(t) + (H(t-t_1) - H(t-t_2))C_{rI}(t) \\ & + H(t-t_2)C_{rs}(t), \end{aligned} \tag{27}$$

where $C_{rf}(t)$, $C_{rI}(t)$ and $C_{rs}(t)$ are the concentration of the radiotracer on the reference region, respectively, for the fast, intermediate and slow stage. $H(t)$ is the Heaviside function defined by

$$H(t-a) = \begin{cases} 0, t < a, \\ 1, t \geq a. \end{cases} \tag{28}$$

$$H(t-a) - H(t-b) = \begin{cases} 0, t < a \text{ and } t \geq b, \\ 1, a \leq t < b. \end{cases} \tag{29}$$

5. Results and discussion

In order to obtain the analytical solution of two-compartment model, Eq. (15) for $[^{11}C]PIB$ and Eq. (24) for $[^{18}F]FDG$ radiotracer, the important step is to determine $C_r(t)$ that will allow you to calculate the input function (Eq. (26)). In the reference region, $C_r(t)$, is approximated by means of linear and nonlinear regression of the data obtained from a discrete TAC curve on a positron emission tomography (PET) image, using PMOD, a biomedical image quantification software.

5.1 $C_r(t)$ for $[^{11}C]PIB$ radiotracer

For $[^{11}C]PIB$ tracer is chosen as reference region the left and right cerebellum, known to be amyloid free illustrated in **Figure 4**. The left and right cerebellum are

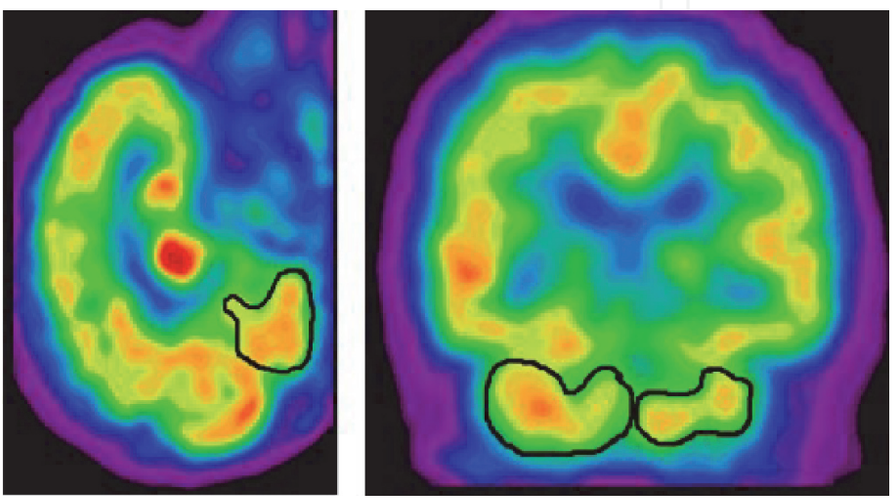

Figure 4.
Region of reference outlined in both cerebellar gray matter in a sagittal (left) and coronal (right) slices.

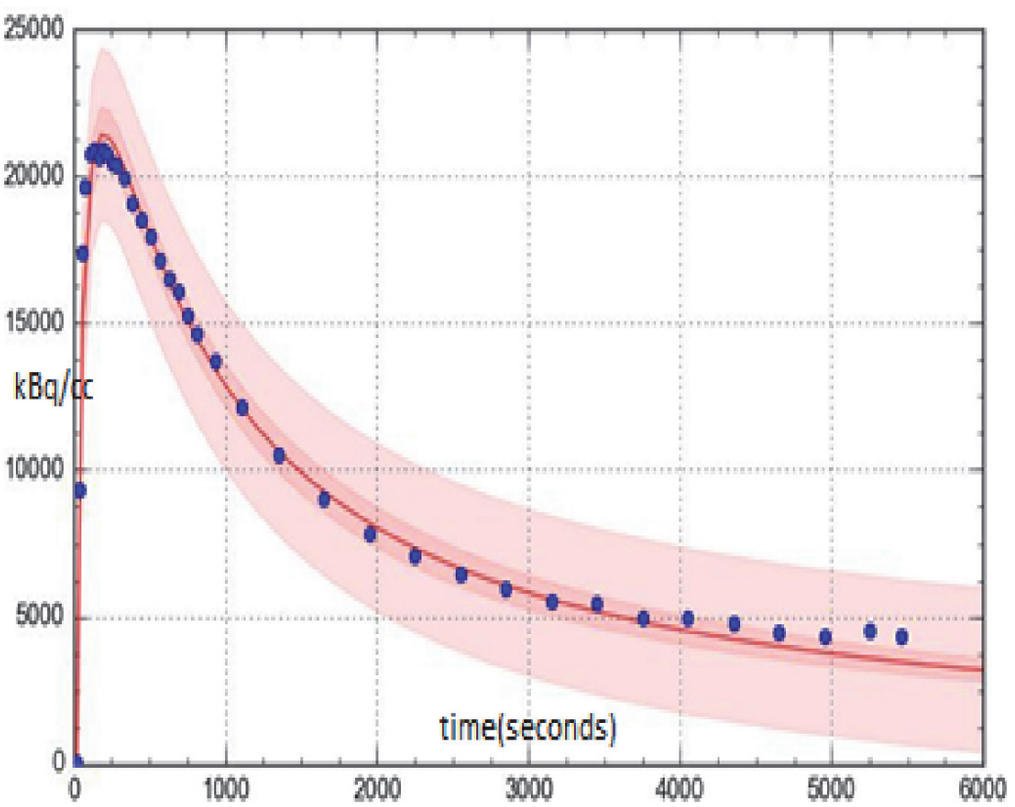

Figure 5.
Discrete and fitted rational cerebellum TAC ($C_r(t)$): the best model.

clearly visible, defined as the discrete left TAC and right TAC, and then the discrete average TAC is generated.

Nonlinear regression is applied to determine the parameters of the model chosen to approximate $C_r(t)$, from a discrete TAC curve.

The rational model (**Figure 5**) showed to be adequate for those seven patients (**Figure 6**), only differentiating by the values of the parameters a, b, c, d.

$$C_r(t) = \frac{at + b}{ct^2 + dt + 1} \tag{30}$$

The technique was applied for 7 patients considering the activity for the reference regions: right cerebellum, left cerebellum, and also for the mean of both (total of 24 simulations). The minor R^2 was 0.96421. The attempt to use an average of all discrete TAC was not to be adequate.

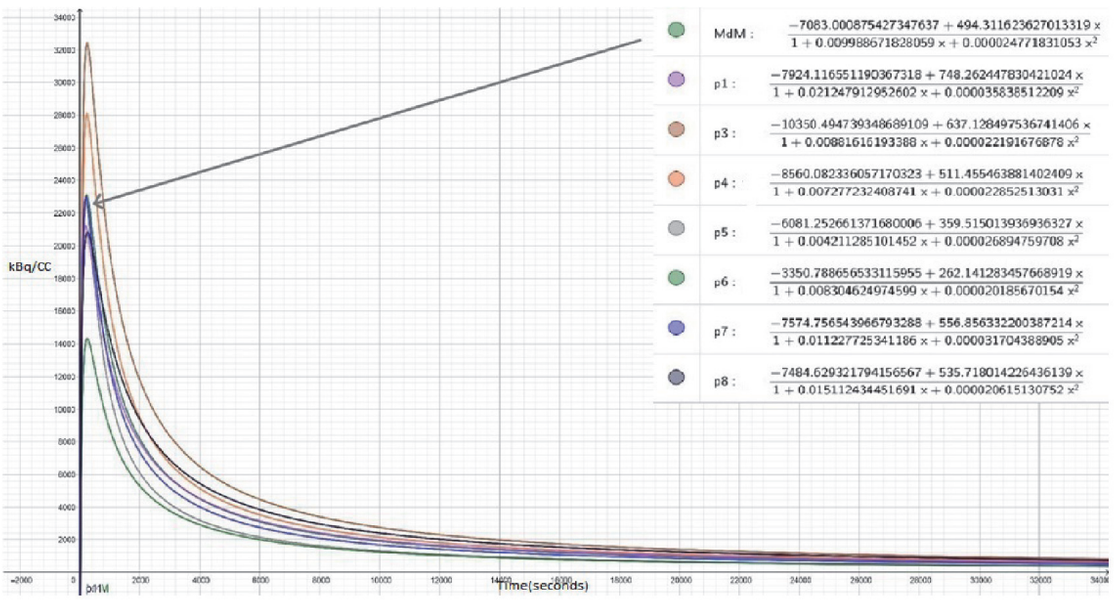

Figure 6.
Average (MdM) and rational fitted cerebellum time active (P1,P3-P8) curve ($C_r(t)$).

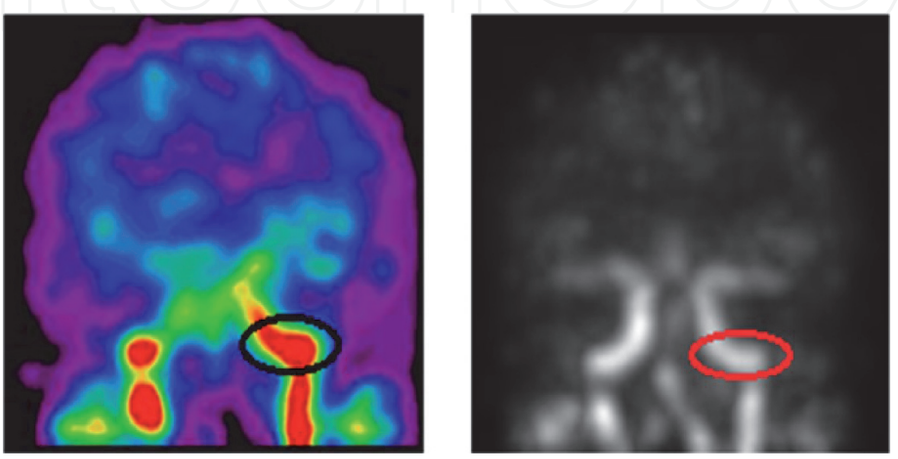

Figure 7.
Region of reference outlined in the left carotid artery region in a coronal slice in both PET (left) and MIP (right) images.

5.2 $C_r(t)$ for $[^{18}F]FDG$ radiotracer

In order to obtain $C_r(t)$ for $[^{18}F]FDG$ radiotracer, the carotids are chosen as reference region. Manually, it is defined as volumes-of-interests (VOIs), illustrated in **Figure 7**, using a biomedical image quantification software PMOD. Over which the left and right carotid arteries where clearly visible, is defined discrete TAC.

Then, it may be appropriate to estimate the $C_r(t)$ considering the fast and slow stage.

After this, we apply regression techniques, and in two stages of the time, a good option that came up was the piecewise function logistical to describe the behavior of

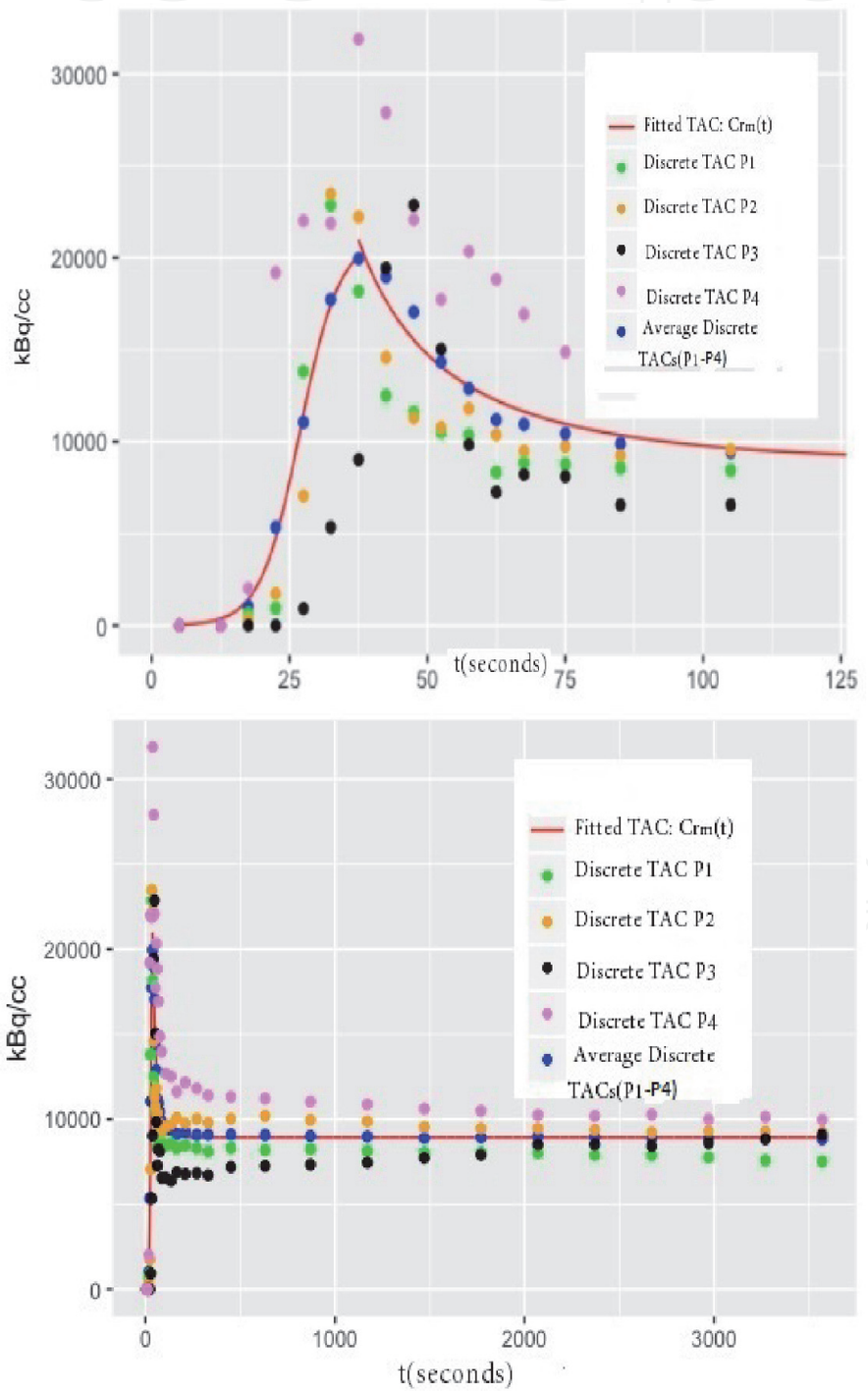

Figure 8.
Discrete TACs (P1–P4) and average logistic fitted carotid TAC ($C_{rm}(t)$) [21].

the mean of the discrete TACs of four patients (considering left volume), **Figure 8**, with correlation coefficient of 0.9947 (at least) is

$$C_r(t) = \frac{[H(t) - H(t - 37.5)]21088.3809}{1 + 1861.3158e^{0.2801t}} + \frac{[H(t - 37.5) - H(t - 3750)]8921.3}{1 - 1.7712e^{0.03t}} \tag{31}$$

It may be convenient in the diagnosis of Alzheimer's disease to consider the specific time interval seconds, [22, 23]. In this time interval, the graphs in **Figure 8** show the comparison between the values estimated by the function and the concentration of the FDG radiotracer in the left VOI. As we can see, the estimated values between 1170 and 2970 s were close to the original values, with the lowest average relative error is 0.0582 and the highest is 0.1096.

6. Conclusion

The aim this study was described the algorithms of kinetic modeling to analyze the pattern of deposition of amyloid plaques and glucose metabolism in Alzheimer's dementia, obtaining the exact solution of the $[^{11}C]PIB$ two-tissue reversible compartment model and a $[^{18}F]FDG$ two-tissue irreversible compartment model. Was solved a system of two first-order differential equations, applying the Laplace transform technique. Many sources of errors are involved in this problem. For example, the gathering data in image processing and the input function construction. With the exception of these errors, is assuring by using Laplace method proposed, there will not be error accumulation.

Longitudinal studies, without arterial blood samples, can assist in the calculation of the dose of medicine, providing the stabilization of cognitive impairment, behavior and the performance of activities of daily living. The technique here described can be used to analyze the pattern of deposition of amyloid plaques, glucose metabolism, the cortical and functional structure of the brain of SuperAgers in relation to cognitively normal elderly and individuals with Alzheimer's dementia. Older adults with exceptional memory ability are coined SuperAgers. Their preserved cognitive capacities with aging may help uncover neuromechanisms of dementia. These individuals showed whole-brain volume similar to middle-aged individuals and some areas thicker than usual agers. Intriguingly, they also exhibited decreased atrophy rate when compared to normal older adults. To our knowledge, their brain functional integrity is yet to be uncovered.

Thanks

This study was made possible by a team work from all members of the SuperAgers project: Lucas Porcello Schilling, Louise Mross Hartmann, Ana Maria Marques da Silva, Cristina Sebastiao Matushita, Mirna Wetters Portuguez, Alexandre Rosa Franco, and Ricardo Bernardi Soder. This research was partially supported by CNPq, project number 403029/2016-3 FAPERGS, project number 27971.414.15498.22062017.

Nomenclature

AIF	arterial input function
CT	computed tomography
EDI	effective dose injected
MIP	maximum intensity projection

PET	positron emission tomography
ROI	region of interest
TAC	time activity curve
VOI	volume of Interest

Author details

Eliete Biasotto Hauser[1,2*], Wyllians Vendramini Borelli[2] and Jaderson Costa da Costa[2]

1 School of Technology, PUCRS, Porto Alegre, Brazil

2 Brain Institute of Rio Grande do Sul (BraIns), PUCRS, Porto Alegre, Brazil

*Address all correspondence to: eliete@pucrs.br

References

[1] Hsieh CH. Positron Emission Tomography Current Clinical and Research Aspects. Croatia: IntechOpen; 2012. pp. 336 DOI: 10.5772/1280

[2] Basu S, Zaidi H, Holm S, Abass A. Quantitative techniques in PET-CT imaging. Current Medical Imaging Reviews. 2011;**7**(3):216-233. DOI: 10.2174/157340511796411186

[3] Borelli WV, Schilling L, Radaelli G, Ferreira L, Pisani L, Portuguez M, et al. Neurobiological findings associated with high cognitive performance in older adults: A systematic review. International Psychogeriatrics. 2018; **30**(12):1813-1825. DOI: 10.1017/S1041610218000431

[4] Borelli WV, Carmona KC, Studart-Neto A, Nitrini R, Caramelli P, da Costa JC. Operationalized definition of older adults with high cognitive performance. Dementia & Neuropsychologia. 2018;**12**(3):221-227. DOI: 10.1590/1980-57642018dn12-030001

[5] Rogalski EJ, Gefen T, Shi J, Samimi M, Bigio E, Weintraub S, et al. Youthful memory capacity in old brains: Anatomic and genetic clues from the northwestern superaging project. Journal of Cognitive Neuroscience. 2013;**25**(1):29-36. DOI: 10.1162/jocn-a-00300

[6] Harrison T, Weintraub S, Mesulam M, Rogalski E. Superior memory and higher cortical volumes in unusually successful cognitive aging. Journal of the International Neuropsychological Society. 2012;**18**(6): 1081-1085. DOI: 10.1017/S1355617712000847

[7] Rodell AB, O'Keefe G, Rowe C, Villemagne V, Gjedde A. Cerebral blood flow and αβ-amyloid estimates by WARM analysis of [^{11}C]PiB uptake distinguish among and between neurodegenerative disorders and aging. Frontiers in Aging Neuroscience. 2017;**8**: 1-11. DOI: 10.3389/fnagi.2016.00321

[8] Zanotti-Fregonara P, Fadaili EM, Maroy R, Comtat C, Souloumiac A, Jan S, et al. Comparison of eight methods for the estimation of the image-derived input function in dynamic [^{18}F]-FDG PET human brain studies. Journal of Cerebral Blood Flow Metabolism. 2009;**29**(11):1825-1835. DOI: 10.1038/jcbfm.2009.9

[9] Laforest R, Sharp TL, Engelbach JA, Fetting NM, Herrero P, Kim J, et al. Measurement of input functions in rodents: Challenges and solutions. Nuclear Medicine and Biology. 2005;**3**: 679-685. DOI: 10.1016/j.nucmedbio.2005.06.012

[10] Zhou S, Chen K, Reiman EM, Li DM, Shan B. A method for generating image-derived input function in quantitative ^{18}F-FDG PET study based on the monotonicity of the input and output function curve. Nuclear Medicine Communications. 2012;**33**(4): 362-370. DOI: 10.1097/MNM.0b013e32834f262e

[11] Su Y, Blazey TM, Snyder AZ, Raichle ME, Hornbeck RC, Aldea P, et al. Quantitative amiloid imaging using image-derived arterial input function. PLoS One. 2015;**10**(4): e0122920. DOI: 10.1371/journal.pone.0122920

[12] Vriens D, de Geus-Oei LF, Oyen WJ, Visser EP. A curve-fitting approach to estimate the arterial plasma input function for the assessment of glucose metabolic rate and response to treatment. Journal of Nuclear Medicine. 2009;**50**(12):1933-1939. DOI: 10.2967/jnumed.109.065243

[13] Chen K, Bandy D, Reiman E, Huang SC, Lawson M, Feng D, et al. Noninvasive quantification of the cerebral metabolic rate for glucose using positron emission tomography, ^{18}F-Fluoro-2-Deoxyglucose, the Patlak method, and an image-derived input function. Journal of Cerebral Blood Flow & Metabolism. 1998;**18**(7):716-723. DOI: 10.1097/00004647-199807000-00002K

[14] Bates DM, Watts DG. Nonlinear Regression and its Applications. New York: Wiley; 1988. pp. 365. DOI: 10.1002/9780470316757

[15] Hauser EB, Venturin GT, Greggio S, Manica E, Zimmer ER, Costa JC. Laplace transform method for ^{11}*C-PIB* two-tissue reversible compartment model with image-derived arterial input function. In: Proceedings of the Ibero Latin American Congress on Computational Methods in Engineering (CILAMCE2017); 5–8 November 2017; Florianopolis. SWGE. 2017. pp. 1-10. DOI: 10.20906/CPS/CILAMCE2017-1077

[16] Hauser EB, Venturin GT, Greggio S, Costa JC. Mathematical modeling to quantify the pharmacokinetic process of [^{18}F]2-fluor-2deoxy-D-glucose (FDG). In: Constanda C, Kirsch A, editors. Integral Methods in Science and Engineering. New York: Birkhäuser; 2015. pp. 301-308. DOI: 10.1007/978-3-319-16727-5-25

[17] Hauser EB, Venturin GT, Greggio S, Borelli WV, Da Costa J. Carotid arterial input function as an inverse problem in kinetic modeling of [^{18}F]2-fluoro-2 deoxy-D-glucose (FDG). Computer Methods in Biomechanics and Biomedical Engineering: Imaging & Visualization. 2019:1-4. DOI: 10.1080/21681163.2019.1647460

[18] Marquardt DW. An algorithm for least-squares estimation of nonlinear parameters. Journal of the Society for Industrial and Applied Mathematics. 1963;**11**:431-441. DOI: 10.1137/0111030

[19] Silva JEM, Furuie SM. Adequacy of compartmental model for positron emission tomography examinations (in Portuguese). Adequação de modelo compartimental para exames de tomografia por emissão de pósitrons. Research on Biomedical Engineering. 2011;**27**(4):231-242. DOI: 10.4322/rbeb.2011.01

[20] Lopresti BJ, Klunk WE, Mathis CA, Hoge JA, Ziolko SK, Lu X, et al. Simplified quantification of Pittsburgh compound B amyloid imaging PET studies: A comparative analysis. Journal of Nuclear Medicine. 2005;**46**(12):1959-1972

[21] Oliveira F. Logistic Model to Describe the Discrete Curves Activities Obtained from PET Images with [^{18}F] FDG Radiotracer at a Carotid Interest (in Portuguese). Modelo Logístico Para Descrever as Atividades de Curvas Discretas Obtidas de Imagens PET Com Radiofárco [^{18}F]FDG Num Volume de Interesse das Carótídas [Dissertation Lato Sensu]. Porto Alegre: PUCRS; 2019

[22] Cunningham VJ, Jones T. Spectral analysis of dynamic PET studies. Journal of Cerebral Blood Flow Metabolism. 1993;**13**(1):15-23. DOI: 10.1038/jcbfm.1993.5

[23] Khalil MM. Basic Sciences of Nuclear Medicine. Berlin: Springer; 2011. pp. 423. DOI: 10.1007/978-3-540-85962-8